Advances in Science and Technology Research Journal

Advances in Science and Technology Research Journal, 2025, 19(10), 150–161
https://doi.org/10.12913/22998624/208317
ISSN 2299-8624, License CC-BY 4.0

Received: 2025.06.25
Accepted: 2025.08.15
Published: 2025.09.01

Comparing adding Co_3O_4 and Fe_3O_4 nanoparticles to improve the performance and emission of biodiesel fuel prepared from waste oils in diesel engines

Qais Hussein Hassan[1], Hayder Abdulkhaleq Alalwan[1*], Alaa Hani Alminshid[2], Malik M. Mohammed[3]

[1] Technical Institute-Kut, Middle Technical University, Baghdad, Iraq
[2] Polymer Research Unit, College of Science, Mustansiriyah University, Baghdad, Iraq
[3] University of Warith Al-Anbiyaa, Karbala, Iraq
* Corresponding author's e-mail: hayder.alalwan@mtu.edu.iq

ABSTRACT

This study examined the effect of adding 50 parts per million [ppm] of either Co_3O_4 or Fe_3O_4 metal-oxide nanoparticles to biodiesel produced from used sunflower oil via transesterification on diesel-engine performance and exhaust pollution reduction. The two powders were first examined using X-ray diffraction, transmission electron microscopy (TEM), and Brunauer-Emmett-Teller (BET) surface area tests. Next, the nanoparticles (NPs) were fed into a four-stroke, single-cylinder engine running at a steady 2500 rpm, and their effect was measured across a range of loads. Measurements included brake-specific fuel consumption (BSFC), brake power (B.P.), brake-thermal efficiency (BTE), brake-specific energy consumption (BSEC), exhaust gases (CO, HC, CO_2, NO_x, and soot), and noise. Adding either NPs improved BSFC by up to 6.6% and 3.3% for cobalt and iron oxides, respectively, and improved efficiency compared to straight biodiesel by 2.7%, 1.4%, respectively. Co_3O_4 outperformed Fe_3O_4, likely because it carries more oxygen and a higher calorific value. Both additives reduced CO and HC by up to 23% and 18%, respectively, yet increased NO_x; Fe_3O_4 caused a smaller increase. Overall, metal-oxide NPs show promise as simple, low-dose boosters for cleaner, more efficient diesel engines.

Keywords: transesterification, biodiesel, nano-powder, engine; emission.

INTRODUCTION

Because it comes from renewable feedstock, biodiesel has caught great interest as a cleaner drop-in replacement for regular diesel fuel [1, 2]. On paper, it boasts a higher cetane number, improved biodegradability, and more oxygen than regular diesel [3]. Those traits help tame engine knock and trim carbon monoxide (CO) and hydrocarbon (HC) output [4]. Yet real-world use still faces several obstacles. As examples, engines can lose efficiency, start sluggishly in the cold, and spit out more nitrogen oxides (NO_x) [5]. Most of these quirks stem from biodiesel's thicker oil film and lower energy content than standard diesel [6, 7].

Over the past few years, researchers and regulators have started to lean heavily on used cooking oils and other waste lipids as the main feedstock for new biodiesel. Tapping this surplus serves two green aims at once: cuts the smoky output of old engines and eases the pressure on municipal waste bins and landfills [8–10]. The go-to recipe for the second-generation fuel remains transesterification, the chemistry that turns oil into biodiesel almost everywhere in the world. At its heart, that reaction simply mixes triglycerides with a short-chain alcohol, often methanol or ethanol, in the presence of a catalyst. People still prefer this approach because the feedstock is renewable, the raw material costs are low, the reaction occurs at mild temperatures, and, crucially,

the final product achieves a cetane number higher than that of regular diesel. One caveat is that the energy per liter comes out a tad lower than the petroleum version [11]. These two points, large emissions gains and a small drop in energy, have made polishing biodiesel's performance an important new goal for labs worldwide.

Adding NPs to the mixture is one bright path researchers are now following [12]. NPs have been used for various applications such as reaction catalysts [13, 14], absorbable materials [15], membranes [16–18], and others [19] due to their unique properties, such as high surface area and reactivity. Particles like cobalt oxide Co_3O_4 or iron oxide Fe_3O_4 show vast surfaces and built-in catalytic sites, so they can quicken the burn, blend air and fuel better, and leave behind less CO and hydrocarbons [20, 21]. The catch is that extra oxygen from the NPs can raise combustion temperature, and that extra heat often enhances the generation of more NO_x [22].

Recently, several studies have looked at adding different NPs to diesel fuels and found that while power and torque usually rise and HC and CO drop, NO_x often climbs sharply. Among the metal oxides, iron oxide, Fe_3O_4, stands out because it conducts heat quickly and, thanks to strong oxygen-iron bonds [23], releases less excess oxygen during combustion than the other oxides, so NO_x growth is less dramatic. Still, direct head-to-head data comparing Fe_3O_4 with cobalt oxide, Co_3O_4, when added to biodiesel from waste sunflower oil, is scarce.

To fill that void, the present work tests both nanoparticle blends in a single-cylinder diesel engine and tracks changes in power, fuel consumption, and exhaust gases. Results of this work show how best to tailor nanotechnology in waste-oil biodiesel for engines that run cleaner while keeping, or even boosting, their performance. This study establishes a strong recommendation to use metal oxide NPs to improve biodiesel performance and emissions.

EXPERIMENTAL WORK

Characterization of Fe_3O_4 and Co_3O_4 NPs

Chosen of commercial Fe_3O_4 (GETNANO, purity 99%) and Co_3O_4 (GETNANO, purity 99.9%) NPs was based on the similarity in their properties, such as particle size and surface area, provided by their vendors. This similarity is important to eliminate the impact of these parameters on the engine performance or emissions. To ensure accurate assessment of the physical and chemical properties of the Fe_3O_4 and Co_3O_4 NPs used in this study, a combination of advanced analytical techniques was employed. Particularly, X-ray diffraction (XRD) analysis (Bruker D8 Advance) was conducted to determine the crystalline structure and phase purity of both metal oxide samples. Transmission electron microscopy (TEM, Hitachi High-Tech, HT7800 Series) was employed to provide detailed information on particle morphology and size distribution, with measurements taken from over 125 randomly selected particles to ensure statistical reliability. The specific surface area of each nanoparticle sample was measured using the BET method, with nitrogen gas serving as the adsorbate as described in previous works [24, 25]. Each BET measurement was triplicated, and the mean value was reported to ensure consistency and reproducibility.

Converting oil to biodiesel

Waste sunflower oil was collected from multiple restaurants and food processing facilities in Baghdad, Iraq. The first step involved filtering the oil to eliminate food residues and other impurities. Subsequently, the transesterification method was employed to convert the oil into biodiesel, chosen for its high efficiency in transforming triglycerides into usable fuel.

To determine the optimal amount of catalyst required for the reaction, a titration was first performed. This involved dissolving 1.2 [g] of potassium hydroxide (KOH, Thermo Fisher, 99.98%) in 1.1 [L] of distilled water to prepare the titrant. For the titration, each 1 [mL] of the oil sample requires 15 [mL] of isopropanol (Thermo Fisher, 99.6% ACS reagent) to dissolve. Using a phenolphthalein indicator (Merck, ACS grade) and 0.1 [N] sodium hydroxide (NaOH, Merck), the mixture was titrated to a pH of 8.5 ± 0.5, carefully adding KOH until a persistent pink color appeared. The volume of KOH consumed was recorded to calculate the required catalyst concentration for neutralizing free fatty acids in the sample.

The transesterification reaction was initiated by mixing the filtered waste sunflower oil with methanol (ACS grade, > 99.8%) at a 6:1 molar ratio (methanol to oil). KOH was added as a catalyst at a concentration of 1% by weight of

the oil, based on literature recommendations for optimal conversion efficiency and minimal soap formation [26–29]. The mixture was stirred magnetically at 650 [rpm] for 5.30 hours at 58 [°C], a temperature below methanol's boiling point to ensure safety and reaction completeness. To promote uniform dispersion of NPs in the biodiesel and prevent their agglomeration, 0.6% sodium dodecyl sulfate (SDS) by weight was included as a surfactant [30, 31].

After the reaction, the mixture was transferred to a covered vessel and allowed to settle for 24 hours, during which glycerol separated from the biodiesel phase. The biodiesel layer was then washed with water and gently heated to 58 [°C] to remove residual moisture. The final biodiesel yield reached approximately 91%, and the product was ready for use.

For the experimental phase, the prepared biodiesel was blended manually with either Co_3O_4 or Fe_3O_4 NPs at a concentration of 50 [ppm]. This dosage was selected based on previous studies, balancing the need for measurable performance improvements to minimize any adverse effects on emissions, particularly NO_x [32–34]. Table 1 presents the characteristics of BID, BIDCo, and BIDFe, where all fuel types were tested at the laboratory of Al-Dorra refinery and compared to those of standard petroleum diesel to assess the impact of nanoparticle additives on fuel properties and engine performance.

Engine tests

To evaluate the influence of nanoparticle-enhanced biodiesel on engine performance and emissions, experiments were conducted using a single-cylinder, four-stroke diesel engine (TD-212, TecQuipment) equipped with pneumatic cooling (Figure 1a) at Middle Technical University. The specification of the engine is listed in previous work [35, 36] and briefly presented in Table 2. The engine was connected to a hydraulic dynamometer and a measurement unit (Figure 1 b), enabling precise control and measurement of torque during testing. Before each test, the engine's fuel tank and supply lines were thoroughly flushed to eliminate any previous fuel and ensure that each test is carried out with only the intended fuel blend. The fuel was supplied directly from the fuel tank to the engine by gravity, where the tank was situated at a higher position compared to the engine.

All tests were conducted at a constant engine speed of 2500 [rpm], which is an average value of engine speed, while varying load conditions (2.0, 4.0, and 6.0 [Nm]), which are most common load values presents during engine run, were used to evaluate performance across different operating scenarios. Each fuel type was assessed under identical conditions to ensure comparability. Before testing, the engine underwent a 10-minute warm-up period to stabilize operating temperatures, guaranteeing consistent results. A dedicated measurement unit continuously recorded key parameters, including torque, speed, and fuel consumption, enabling precise calculation of brake-specific fuel consumption (BSFC), BTE, and brake-specific energy consumption (BSEC). By maintaining standardized testing conditions and controlling variables such as speed and load, the study ensured that any observed variations in performance or emissions were solely attributable to the effects of NPs rather than external influences.

Tested parameters

Several key parameters were measured during the experiments. These included BSFC [g/kWh], which was calculated as the ratio of the fuel consumption rate to the brake power output (B.P., [kW]), following Equation 1. In addition, brake power [kW], which was determined using the engine speed (N, [rpm]) and the torque (T, [Nm]) provided by the dynamometer, as shown in Equation 2. The torque value determined from this step is used to find the BSFC value. Also, BTE was derived from the ratio of brake power to the

Table 1. Properties of the three fuel types

Diesel	Density [g/cm^3]	Viscosity [cSt] at 40	CV [MJ/kg]	Cetane #	LHV [MJ/kg]	Latent heat of vaporization [MJ/kg]
Petroleum diesel	0.80–0.84	2.2–2.5	40.0–45.0	50.0–55.0	40.0–45.0	0.23–0.25
BID	0.879	4.490	39.16050	60.10	37.50	0.2540
BIDCo	0.880	4.500	39.24540	60.50	38.15	0.2550
BIDFe	0.881	4.510	39.25340	60.50	38.30	0.2555

Table 2. Engine technical criteria

Max. power	3.5 [Kw] at 3600 [rpm]
Max. torque	16 [Nm] at 3600 [rpm]
Cylinder radius	34.5 [mm]
Capacity	232 [cm^3]
Connecting rod length	104 [mm]

energy input from the fuel, utilizing the calorific value (CV [kJ/kg]) as shown in Equation 3. Finally, BSEC [MJ/kWh] was obtained by multiplying BSFC by the lower heating value (LHV, [MJ/kg]) as shown in Equation 4 [37, 38]. In Equation 1, $m°f$ represents the hourly fuel consumption [g/h]. After repeating the measurements three times, the mean values were adopted in this study and the error bars were calculated based on the standard error, which indicates the range within which the true value of a measurement is likely to fall.

$$BSFC = \frac{m°f}{B.P.} \quad (1)$$

$$B.P = \frac{2\pi NT}{60000} \quad (2)$$

$$BTE = \frac{B.P.\times 3600}{mof \times CV} \quad (3)$$

$$\text{BSEC} = \text{BSFC} \times LHV \quad (4)$$

Inspection of emission and noise level

To identify the effect of NPs on the environmental performance of biodiesel, both gaseous and particulate emissions were measured during engine operation. A gas analyzer (AIRREX HG-540, Fig. 1c was used to monitor concentrations of the emitted gases, including HC, CO, CO_2, and NO_x. The analyzer was connected directly to the engine's exhaust system via a dedicated pipe, ensuring accurate and real-time sampling of the emitted gases.

For quantifying particulate matter (PM), exhaust was passed through 934-AH borosilicate

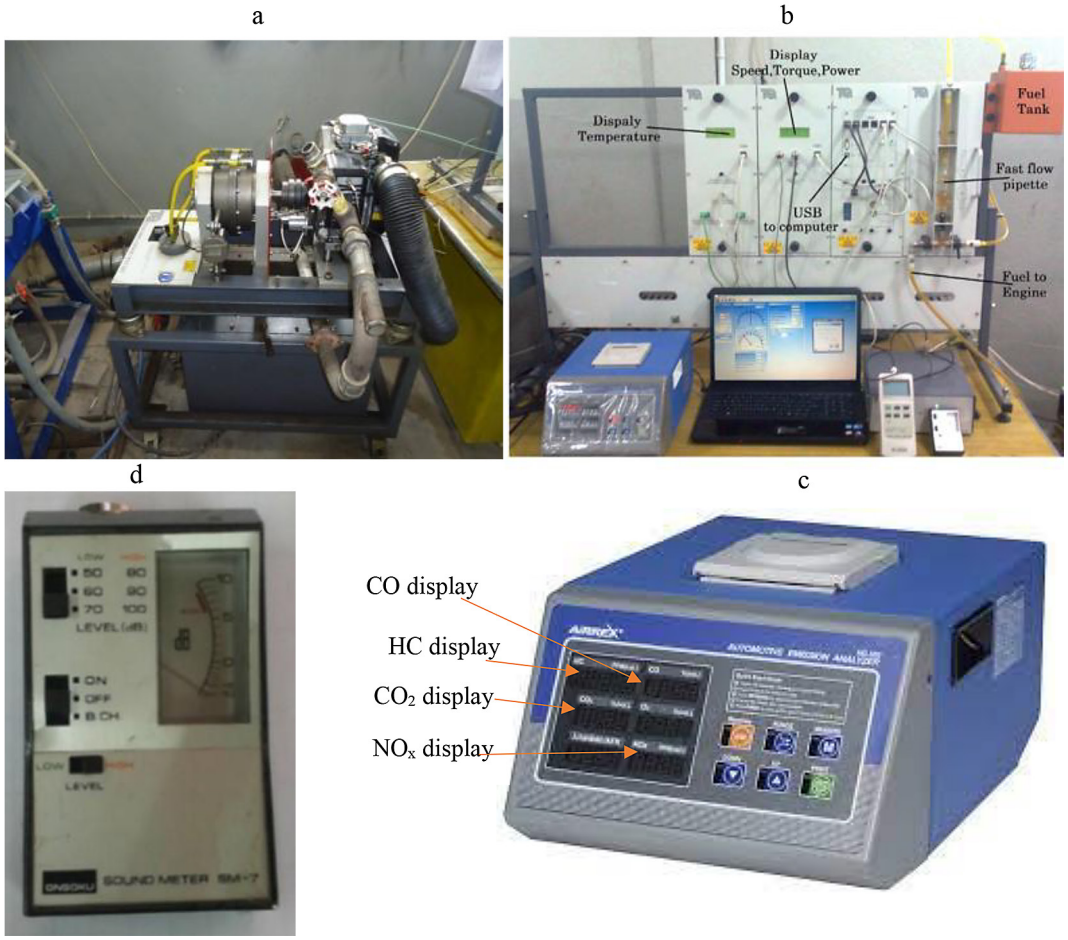

Figure 1. Equipment used in this work to analyze the engine performance and emission (a) the engine, (b) the measurement unit, (c) the AIRREX HG-540 emission analyzer, and (d) sound pressure level meter

glass fiber filters. Each filter was weighed before and after the test, runs to determine the mass of particulates collected during engine operation. All emission measurements were conducted in triplicate, and the mean values were reported to enhance data reliability.

Noise levels were also evaluated for each fuel blend under all tested load conditions. A sound pressure level meter (Figure 1 d) was used to record noise in decibels [dB], with four microphones positioned one meter away from the engine on all sides – front, back, left, and right – to capture a comprehensive profile of sound emissions. This arrangement ensured that noise measurements reflected the overall acoustic impact of the engine during operation with different fuel blends.

RESULTS AND DISCUSSION

Characterization of NPs

The structural and morphological features of the Co_3O_4 and Fe_3O_4 NPs were thoroughly examined using a suite of advanced characterization techniques. X-ray diffraction (XRD) analysis confirmed that each sample was composed of a single crystalline phase; with Co_3O_4 corresponding to the cubic reference diffraction pattern (JCPDS card 00-042-1467) and Fe_3O_4 matching JCPDS card 01-075-0449. These results indicate the presence of the only pure phase in the used samples [24, 25]. TEM images show that the NPs are similar in morphology and size, with Co_3O_4 exhibiting an average diameter of 50 ± 5 [nm] and Fe_3O_4 averaging 50 ± 7 [nm]. The specific surface areas, determined by the BET method, were found to be 19.0 ± 1 [m²/g] for Co_3O_4 and 18 ± 2 [m²/g] for Fe_3O_4. These results confirm the close resemblance in particle size, shape, and surface area between the two types of NPs. This similarity is ensures that any observed differences in engine performance and emissions is attributed to the intrinsic chemical and catalytic properties of the NPs rather than disparities in their physical characteristics.

Engine performance

This research evaluated the efficiency of biodiesel derived from waste oil, both before and after incorporating 50 [ppm] of either Co_3O_4 or

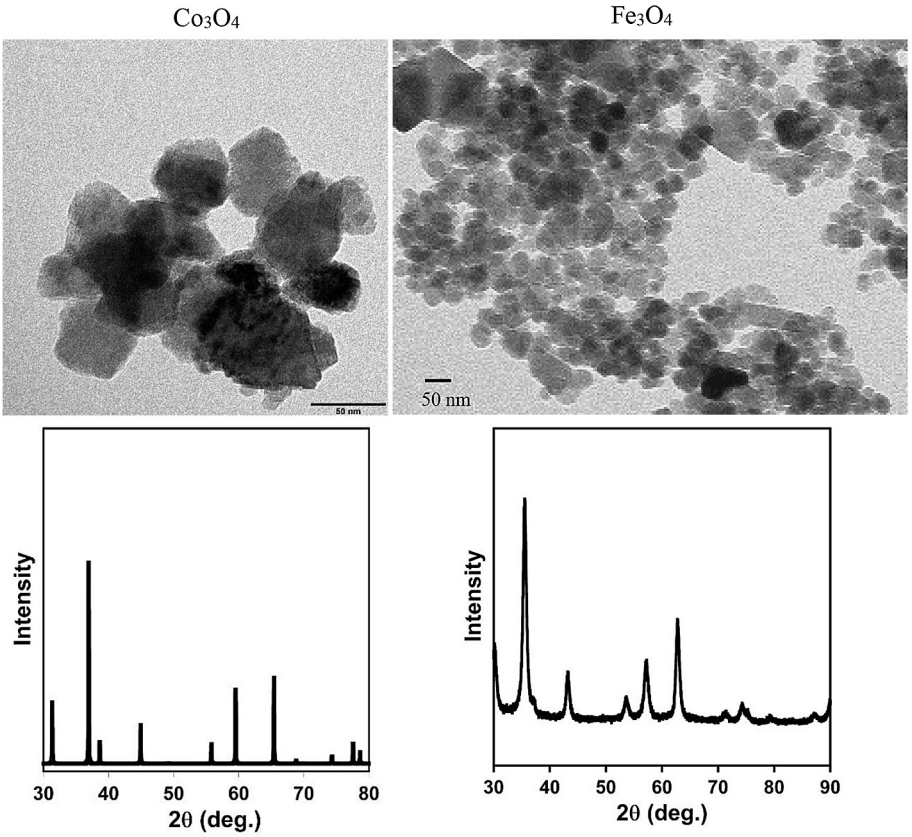

Figure 2. XRD and TEM images of Co_3O_4 and Fe_3O_4 NPs

Fe_3O_4 NPs, using a four-stroke engine as the testing platform. Figure 3a illustrates BSFC for each sample, a metric that measures how much fuel is consumed to generate a unit of power, thus serving as an indicator of fuel efficiency

The findings indicate that the biodiesel sample without NPs (BID) exhibited a higher BSFC compared to those with nanoparticle additives. Lower BSFC indicates better fuel performance regarding fuel consumption. At a torque of 2.0 [Nm], the BSFC values recorded were 620 [g/kWh] for BID, 579 [g/kWh] for the sample with Co_3O_4 (BIDCo), and 599 [g/kWh] for the sample with Fe_3O_4 (BIDFe). The reduction in BSFC upon adding NPs is attributed to the increased oxygen content provided by the nano-additives [39], which enhances combustion efficiency. This trend persisted across all tested load conditions. For instance, at 4.0 [Nm], the BSFC values for BID, BIDCo, and BIDFe were 359, 339, and 349 [g/kWh], respectively. When the torque was raised to 6.0 [Nm], the corresponding BSFC values were 309, 290, and 300 [g/kWh].

BIDCo consistently demonstrated lower BSFC values than BIDFe at every torque level, which is likely due to the higher calorific value and greater oxygen availability from Co_3O_4, facilitating more effective combustion compared to Fe_3O_4. The stronger Fe-O bond relative to the Co-O bond influences the difference in oxygen donation.

As shown in Figure 3(b), the improvement percentage in BSFC for BIDCo and BIDFe at 2.0 [Nm] were 6.6% and 3.3%, respectively. At a higher load of 4.0 [Nm], these improvement slightly decreased to 5.5% for BIDCo and 2.8% for BIDFe, a change attributed to increased fuel consumption at moderate loads [40]. When the torque was further increased to 6.0 [Nm], the improvement percentages were 6.5% for BIDCo and 2.9% for BIDFe, with the limited reduction expected as the torque approached its maximum value.

BSEC serves as a key metric for assessing how effectively an internal combustion engine converts fuel energy into mechanical power output [41]. Lower BSEC values indicate improved energy conversion efficiency, making it a valuable parameter for comparing different fuel formulations and engine modifications.

Experimental results demonstrate that introducing NPs into BID leads to a reduction in BSEC across all tested torque levels, with the most pronounced decrease observed at the highest load of 6 [Nm]. For BID alone, the BSEC values at torque settings of 2.0, 4.0, and 6.0 [Nm] are 23.249, 13.529, and 11.625 [MJ/kWh], respectively. The addition of NPs not only raises the lower heating value (LHV) of the fuel but also lowers the BSFC, resulting in lower BSEC values for nanoparticle-enhanced biodiesel. Specifically, BIDCo exhibits BSEC values of 22.15, 12.99, and 10.99 [MJ/kWh] at 2.0, 4.0, and 6.0 [Nm], respectively, while BIDFe records 22.91, 13.40, and 11.40 [MJ/kWh] at the same torque levels.

BIDCo consistently shows higher loss percentages than BIDFe: 4.7% versus 1.5% at 2 [Nm], 4.0% versus 0.84% at 4 Nm, and 5.1% versus 2.2% at 6 [Nm]. These findings indicate that the inclusion of NPs significantly reduces the BSEC loss, with Co_3O_4 NPs outperforming Fe_3O_4 NPs due to their greater oxygen content and the higher LHV of the BIDCo blend.

Figure 5 illustrates the BTE for each fuel type at three different torque settings, revealing that the BTE values are generally comparable, particularly after the inclusion of NPs. Despite this overall similarity, BTE increases noticeably with higher torque for all fuels, a trend attributed to reduced fuel consumption at elevated torque levels. BTE is a crucial metric for assessing how

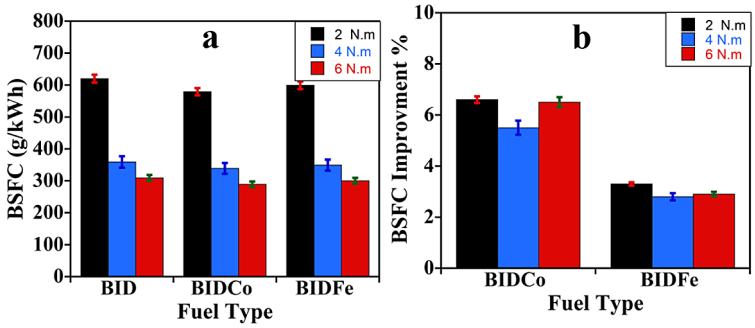

Figure 3. (a) BSFC values of and (b) the BSFC's improvement percentages compared to BID

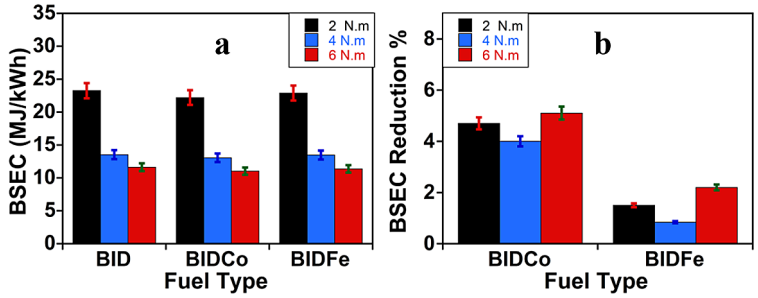

Figure 4. (a) BSEC values of the three tested fuels and (b) reduction percentage of BSEC compared with BID

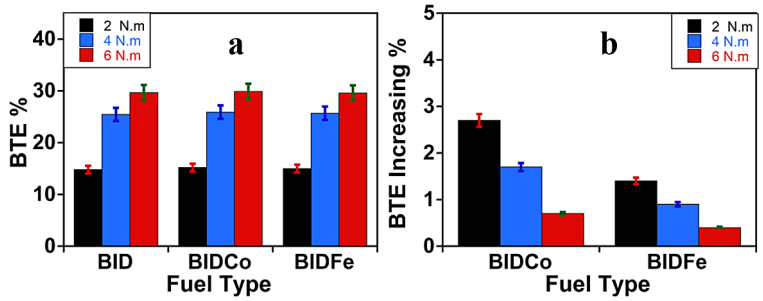

Figure 5. (a) BTE values of the three tested fuels and (b) BTE increasing percentage relative to BID

effectively an engine transforms the chemical energy in fuel into mechanical work. Energy losses during this process can arise from factors like friction, emitted gases, and heat dissipation through the engine cylinder [42]. The observed enhancement in BTE following the addition of NPs is primarily due to the increased calorific value and reduced viscosity of the fuel, which together promote improved fuel flow and combustion that is more efficient.

In more detail, at 2.0, 4.0, and 6.0 [Nm], the BTE levels of BID are 14.79, 25.45, and 29.66, respectively. Incorporating Co_3O_4 NPs raises these values to 15.19, 25.89, and 29.88 at the same torque levels, while with Fe_3O_4 NPs, the BTE values become 14.98, 25.69, and 29.78, respectively. As shown in Figure 5(b), the degree of BTE improvement diminishes as the load increases, which is linked to lower fuel consumption at higher loads. The most significant gains are observed with Co_3O_4 NPs, where at 2.0, 4.0, and 6.0 [Nm], BTE increases by 2.7%, 1.7%, and 0.7%, respectively. For Fe_3O_4 NPs, the corresponding improvements are 1.4%, 0.9%, and 0.4%. These results indicate that Co_3O_4 NPs are more effective in enhancing engine performance and fuel efficiency, while Fe_3O_4 NPs also offer benefits, particularly in reducing NO_x emissions, which will be addressed in subsequent sections.

As the applied torque increases, the noise level also rises, as shown in Figure 6. For the BID sample, noise measurements at 2.0, 4.0, and 6.0 [Nm] were recorded as 74, 76, and 78 [dB], respectively. Introducing NPs led to a marked decrease in noise. Specifically, BIDCo exhibited noise levels of 72.0, 73.0, and 74.0 [dB] at the same torque values, while BIDFe showed 73, 75, and 76 [dB]. This decrease is assigned to the enhanced of O_2 availability during combustion when Co_3O_4 and Fe_3O_4 NPs are present. Co_3O_4 provides more accessible oxygen than Fe_3O_4, resulting in superior noise reduction performance for BIDCo compared to BIDFe.

Exhaust emissions

Figure 7 presents the engine's emission data both before and after the incorporation of NPs into the fuel. In general, increasing the applied load leads to higher release of certain emissions, such as PM and HC, due to a shortened combustion duration that promotes their formation. Conversely, higher loads raise the temperature, which reduces CO emissions by limiting incomplete combustion and enhancing complete combustion, thereby increasing CO_2 and NO_x emissions [43].

The figure also illustrates a clear decrease in HC, CO, and PM emissions when NPs,

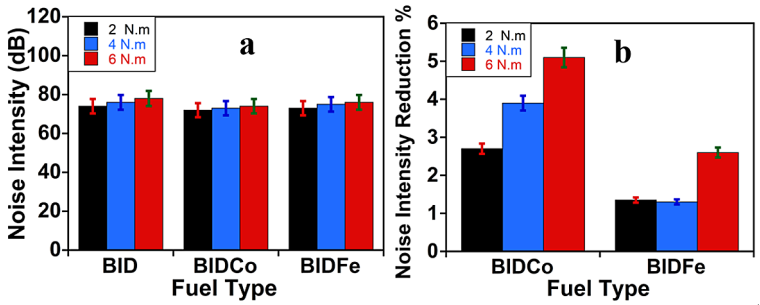

Figure 6. (a) The intensity of engine noise in dB of the three tested fuels and (b) the reduction percentages based on BID

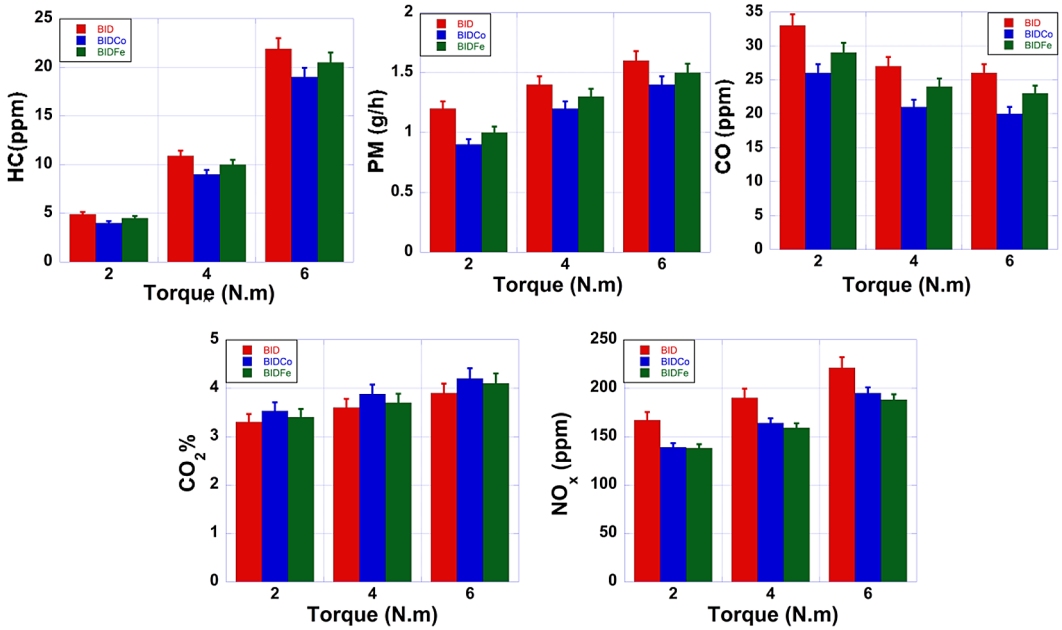

Figure 7. The emissions of the three tested fuels from the exhaust

particularly Co_3O_4, are added to BID fuel. However, as the load increases, emissions of NO_x and CO_2 also rise. Figure 8 quantifies the percentage reductions in PM, CO, and HC achieved by the nano-additive BID across various load levels. More in detail, HC releasing levels for BID at 2.0, 4.0, and 6.0 [Nm] are measured at 4.9, 10.9, and 21.9 [ppm], respectively, while for BIDFe they are 18%, 17.0%, and 13%, respectively. This means that the reduction percentages of BIDFe are 8%, 7.9%, and 2.0%, respectively. The better performance of BIDCo is due to its easy donation of oxygen compared to Fe_3O_4.

Similarly, CO emission was reduced after the addition of BIDCo by 18%, 22%, and 23% at load value 2.0, 4.0, and 6.0 [Nm], respectively, while it was 12%, 11%, and 12%, respectively, for BIDFe. In addition, PM releasing levels of BID are 1.2, 1.4, and 1.6 [g/h], respectively, but the use of BIDCo and BIDFe further reduces them. Specifically, for BIDCo, it was 0.9, 1.1, and 1.2 [g/h], respectively, and for BIDFe was 1.1, 1.3, and 1.5 [g/h], respectively. This denotes that BIDCo decreases PM release at 2.0, 4.0, and 6.0 [Nm] by about 25%, 14%, and 12%, respectively, while BIDFe reduces it by 16%, 7%, and 6.25%, respectively.

HC and PM emissions result from the poor combustion of fuel in the combustion and evaporation steps [44]. Thus, the high reduction in HC and PM emissions after the addition of NPs is attributed to the better fuel combustion as a result of the higher available oxygen of BIDCo and BIDFe [45]. The physicochemical properties of fuel have a strong impact on combustion emissions, where the low available oxygen leads to a

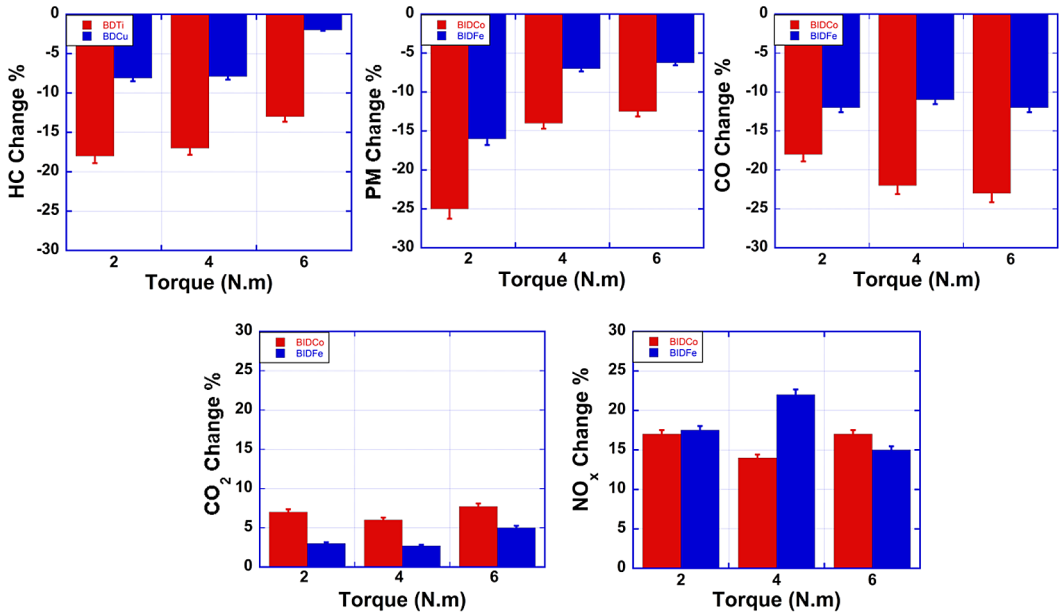

Figure 8. The emission variation percentages of the three tested fuels

rise in CO release because of the enhancement of partial oxidation rather than complete combustion. Thus, BID-NPs minimize CO emissions due to their higher oxygen content [46].

The noticeable rise in CO_2 release is due to the reduction of PM, HC, and CO emissions. Compared to BID fuel, BID-NPs fuel promotes more complete oxidation and reduces partial oxidation, resulting in lower emissions of HC, CO, and PM. The simultaneous rise in CO_2 alongside the reduction in these pollutants indicates more efficient and complete fuel combustion. Additionally, higher engine temperatures at increased loads contribute to this effect. Moreover, the presence of NPs enhances the fuel combustion process compared to BID alone, which further elevates CO_2 emissions [47].

The increase in NO_x emissions clearly reflects the effect of higher combustion temperatures on pollutant formation [48]. NO_x is generated through the reaction between oxygen, either from NPs, biofuel, or air, and nitrogen present in the air. Elevated combustion temperatures and greater oxygen availability enhance this process. For example, before adding NPs, NO_x concentrations at 2.0, 4.0, and 6.0 [Nm] were measured at 167.0, 190, and 221 [ppm], respectively. After introducing NPs, NO_x emissions from Fe_3O_4 were lower than those from Co_3O_4, likely due to Fe_3O_4's reduced capacity to supply oxygen for combustion compared to Co_3O_4. Specifically, NO_x levels for BIDCo at 2.0, 4.0, and 6.0 [Nm] were 139, 164, and 194 [ppm], while BIDFe recorded 138.0, 159.0, and 188.0 [ppm] at the same loads. This corresponds to NO emission reductions of 16.7%, 14.2%, and 16.7% for BIDCo, and 17.3%, 21.5%, and 14.9% for BIDFe at 2.0, 4.0, and 6.0 [Nm], respectively.

Their distinguished properties, features, and catalytic behaviors in the fuel burning process can demonstrate the variation in CO_2 and NO_x releases observed with Co_3O_4 and Fe_3O_4 NPs. In particular, Co_3O_4 is recognized for its strong oxidizing capability, which promotes diesel combustion, driving to higher burning temperatures inside the engine [49, 50]. This rise in combustion temperature enhances the interaction between N_2 and O_2, the main components of air, and elevates NO_x release. Besides that, although the elevated denoted oxygen of Co_3O_4 compared to Fe_3O_4 leads to enhanced full combustion, it produces more NO_x because of the elevated thermal level. In contrast, Fe_3O_4 has various thermal properties and a slashes propensity to increase undue heat production compared to that of Co_3O_4. As mentioned before, Fe_3O_4's ability to influence the heat transfer from the burning cell to the exhaust allows lowering peak temperatures, thereby reducing NO_x emissions.

To confirm the important effect of adding NPs to BID, all the results in sections (3.2.) and (3.3.) were analyzed statistically via analysis of variance (ANOVA). This analysis method is ordinarily applied to test the variation between the mean

values of more than two groups. ANOVA results show values less than 0.05 for all calculated P parameter values, which indicates that all observed improvements are considerable and respectable and are not just random scatter, which gives high credibility to these study results.

The potential for expanding this method on a larger scale relies on carefully weighing the associated expenses against the benefits, particularly in terms of modulating fuel activity and lower releases. From an environmental perspective, utilizing waste oil as a raw material for BID is advantageous, as it encourages recycling and minimizes garbage generation. Nevertheless, incorporating NPs does result in higher fuel costs. Initially, the investment required for producing NPs may be significant; however, these upfront costs could be balanced out over time by the gains in fuel efficiency and the reduction of emissions. Furthermore, with increasingly stringent emission regulations, there is a growing appeal for green fuels, thereby enhancing the economic justification for adding NPs to biodiesel.

Regarding environmental sustainability, biodiesel enhanced with NPs offers notable benefits compared to other sustainable liquid fuels, particularly by decreasing the release of harmful substances like HC, CO, and PM. Although there is a rise in CO_2 emissions, it is accompanied by a reduction in the more hazardous CO gas. On the other hand, the common challenge with using biodiesel is its tendency to produce higher levels of NO_x compared to conventional diesel fuel due to the high oxygen content of biodiesel. The findings indicate that Fe_3O_4 NPs are less promoting to NO_x gases compared to Co_3O_4.

CONCLUSIONS

This study shows that the addition of metal oxide NPs (Co_3O_4 and Fe_3O_4) to biodiesel produced from waste sunflower oil can significantly enhance diesel engine performance and emission characteristics. Particularly, the addition of 50 [ppm] of either NPs into biodiesel results in a notable reduction in BSFC across all tested load conditions, with Co_3O_4 showing better performance due to its higher calorific value and ability to transfer more oxygen molecules, resulting from its weaker oxygen bond compared to Fe_3O_4. In addition, both NPs improved BTE and reduced emissions of CO, PM, and HC compared to BID.

However, the use of NPs was associated with a moderate increase in NO_x emissions, a common challenge when enhancing combustion efficiency with oxygen-rich additives. Notably, Fe_3O_4 exhibited a less pronounced increase in NO_x emissions than Co_3O_4 due to its lower oxygen donation capability and higher thermal conductivity, which results in heat transfer away from the combustion chamber.

The results confirm that NPs, particularly Co_3O_4, are effective in solving most of the drawbacks of biodiesel regarding engine efficiency and emissions, making them promising additives for sustainable diesel engine operation. However, future work should focus on optimizing nanoparticle concentrations, exploring long-term engine durability, and developing strategies to mitigate NO_x emissions to further advance the practical application of nanoparticle-enhanced biodiesel fuels.

REFERENCES

1. As'ad S., Alsaqoor S., Al-Busoul M.A.A., Abu-Zaid M., Joka-Yilidz M., Borowski G., Al-Khawaldeh M.A. Performance comparison of four-stroke diesel engine fuelled by various biodiesel blends and diesel, Advances in Science and Technology. Research Journal, 2023; 17.
2. Lotko W., Smigins R., Tziourtzioumis D., Górska M. Environmental aspects of a common rail diesel engine fuelled with biodiesel/diesel blends, Advances in Science and Technology. Research Journal, 2022; 16: 192–201.
3. Shaker F.N., Obed A.A., Abid A.J., Saleh A.L., Hassoon R.J. Energy management strategy for PV PSO MPPT/fuel cell/battery hybrid system with hydrogen production and storage, Journal of Techniques, 2023; 5: 52–60.
4. Mohammed A.S., Atnaw S.M., Ramaya A.V., Alemayehu G. A comprehensive review on the effect of ethers, antioxidants, and cetane improver additives on biodiesel-diesel blend in CI engine performance and emission characteristics, Journal of the Energy Institute, 2023; 101227.
5. Zangana L.M.K., Yaseen A.H., Hassan Q.H., Mohammed M.M., Mohammed M.F., Alalwan H.A. Investigated kerosene-diesel fuel performance in internal combustion engine, Cleaner Engineering and Technology, 2023; 12: 100591.
6. Gautam R., Kumar S. Performance and combustion analysis of diesel and tallow biodiesel in CI engine, Energy reports, 2020; 6: 2785–2793.

7. Saxena V., Kumar N., Saxena V.K. Combustion, performance and emissions of *Acacia concinna* biodiesel blends in a diesel engine with variable specific heat ratio, Journal of Thermal Analysis and Calorimetry, 2021; 1–18.
8. Casas L.C., Orjuela A., Poganietz W.-R. Sustainability assessment of the valorization scheme of used cooking oils (UCOs): the case study of Bogotá, Colombia, Biomass Conversion and Biorefinery, 2024; 14: 15317–15333.
9. Vlachokostas C. Closing the loop between energy production and waste management: A conceptual approach towards sustainable development, Sustainability, 2020; 12: 5995.
10. Le T.T., Tran M.H., Nguyen Q.C., Le H.C., Cao D.N., Paramasivam P. Nanotechnology-based biodiesel: a comprehensive review on production, and utilization in diesel engine as a substitute of diesel fuel, International Journal of Renewable Energy Development, 2024; 13: 405–429.
11. Govindhan P., Prabhu N., Edison Chandraseelan R., Dharmendira Kumar M. Technologies of bio-diesel production: A state of the art review, Petroleum Science and Technology, 2024; 42: 339–356.
12. Bitire S.O., Nwanna E.C., Jen T.-C. The impact of CuO nanoparticles as fuel additives in biodiesel-blend fuelled diesel engine: A review, Energy & Environment, 2023; 34: 2259–2289.
13. Mohammed M.M., Ali N.S.M., Alalwan H.A., Alminshid A.H., Aljaafari H.A. Synthesis of ZnO-CoO/Al_2O_3 nanoparticles and its application as a catalyst in ethanol conversion to acetone, Results in Chemistry, 2021; 3: 100249.
14. Alalwan H.A., Alminshid A.H., Mohammad M., Hussein S.A.M., Mohammed M.F. Employing synthesized MgO-SiO_2 nanoparticles as catalysts in ethanol conversion to 1, 3-Butadiene, International Journal of Nanoscience and Nanotechnology, 2022; 18: 157–166.
15. Mohammed M.M., Alalwan H.A., Alminshid A., Hussein S.A.M., Mohammed M.F. Desulfurization of heavy naphtha by oxidation-adsorption process using iron-promoted activated carbon and Cu+ 2-promoted zeolite 13X, Catalysis Communications, 2022; 106473.
16. Beauregard N., Al-Furaiji M., Dias G., Worthington M., Suresh A., Srivastava R., Burkey D.D., McCutcheon J.R. Enhancing iCVD modification of electrospun membranes for membrane distillation using a 3D printed Scaffold, Polymers, 2020; 12: 2074.
17. Kalash K.R., Al-Furaiji M.H., Waisi B., Ali R.A. Evaluation of adsorption performance of phenol using non-calcined Mobil composition of matter no. 41 particles, Desalin. Water Treat., 2020; 198: 232–240.
18. Al-Musawy W.K., Al-Furaiji M.H., Alsalhy Q.F. Synthesis and characterization of PVC-TFC hollow fibers for forward osmosis application, Journal of Applied Polymer Science, 2021; 138: 50871.
19. Shadhar M.H., Salih B.M.M., Khaleel O.R., Kadhim Y.M., Mohammed M.M., Alalwan H.A. The influence of eggshell nanoparticles as a partial replacement of cement in concrete, Innovative Infrastructure Solutions, 2024; 9: 465.
20. Balasubramanian D., Gnanavel J.R.S., Venugopal I.P., Wu H.-W. Enhanced combustion characteristics of diesel, biodiesel blends infused with cobalt oxide nanoparticles: droplet-scale experimentation and flame analysis, Combustion Science and Technology, 2025; 1–44.
21. Mohammad S.I.S., Vasudevan A., Prasad K.D.V., I.R. Ali, Kumar A., A. Kulshreshta, V.S. Mann, I.B. Sapaev, T. Kalyani, M. Sina, Evaluation of diesel engine performance and emissions using biodiesel from waste oils synthesized with Fe_3O_4-SiO_2 heterogeneous nano catalyst, Heliyon, 2025; 11.
22. Hussain J., Mubarak M., Boopathi D., Jayabal R. A comprehensive review of production and utilisation of ammonia as potential fuel for compression ignition engines, Next Sustainability, 2025; 5: 100116.
23. Lu J., Liu Q., Xiong Z., Xu Z., Cai Y., Wang Q. Activation of peroxymonosulfate with magnetic and recyclable Fe_3O_4@ C/$MnCo_2O_4$ nanocomposites for the decolorization of Acid Orange II, Journal of Chemical Technology & Biotechnology, 2017; 92: 1601–1612.
24. Alalwan H.A., Alminshid A., Mohammed M.M., Mohammed M.F. Spectroscopic Investigation of Carbon Dioxide Interactions with Transition Metal-Oxide Nanoparticles, Chemical Engineering & Technology, 2023; 46: 587–594.
25. Alalwan H.A., Alminshid A.H., Mohammed M.M., Mohammed M.F. Methane activation on metal oxide nanoparticles: spectroscopic identification of reaction mechanism, Particulate Science and Technology, 2022; 1–8.
26. Sanli H., Canakci M. Effects of different alcohol and catalyst usage on biodiesel production from different vegetable oils, Energy & Fuels, 2008; 22: 2713–2719.
27. Demirbas A. Relationships derived from physical properties of vegetable oil and biodiesel fuels, Fuel, 2008; 87: 1743–1748.
28. Rashid U., Anwar F. Production of biodiesel through optimized alkaline-catalyzed transesterification of rapeseed oil, Fuel, 2008; 87: 265–273.
29. Hassan Q.H., Araibi A.S., Shather A.H., Mohammed M.M., Alalwan H.A. The impact of utilizing waste sunflower oil as a biodiesel blend on four-stroke engine performance and emissions, Designs, 2024; 8: 38.
30. Soudagar M.E.M., Nik-Ghazali N.-N., Kalam M.A., Badruddin I.A., Banapurmath N., Khan T.M.Y., Bashir M.N., Akram N., Farade R., Afzal A. The

effects of graphene oxide nanoparticle additive stably dispersed in dairy scum oil biodiesel-diesel fuel blend on CI engine: performance, emission and combustion characteristics, Fuel, 2019; 257: 116015.

31. Soudagar M.E.M., Nik-Ghazali N.-N., Kalam M.A., Badruddin I.A., Banapurmath N.R., Akram N. The effect of nano-additives in diesel-biodiesel fuel blends: A comprehensive review on stability, engine performance and emission characteristics, Energy conversion and management, 2018; 178: 146–177.
32. Mujtaba M.A., Kalam M.A., Masjuki H.H., Gul M., Soudagar M.E.M., Ong H.C., Ahmed W., Atabani A.E., Razzaq L., Yusoff M. Comparative study of nanoparticles and alcoholic fuel additives-biodiesel-diesel blend for performance and emission improvements, Fuel, 2020; 279: 118434.
33. Sathish T., Saravanan R., Rajasimman M., Ghfar A.A., Ramkumar V. Nanoparticle assorted biofuels production from biowastes through transesterification, Fuel, 2023; 331: 125875.
34. Ansari A.M., Memon L.A., Ghannam M.T., Selim M.Y. Impact of biodiesel blended fuel with nanoparticles on performance and noise emission in compression ignition engine, International Journal of Thermofluids, 2023; 19: 100390.
35. Hassan Q.H., Ali N.S.M., Alalwan H.A., Alminshid A.H., Mohammed M.M. The impact of adding nanoparticles to biodiesel fuel prepared from waste sunflower oil on the performance and emission of diesel engines, Circular Economy, 2025; 4: 100138.
36. Hassan Q.H., Alalwan H., Mohammed M., Mohammed M.F. Identifying the impact of methanol-diesel fuel on the environment using a four-stroke ci engine, Journal of Applied Engineering Science, 2023; 1–6.
37. Bayraktar H. An experimental study on the performance parameters of an experimental CI engine fueled with diesel–methanol–dodecanol blends, Fuel, 2008; 87: 158–164.
38. Maniyath S., Rajan R., Vaisakh S., Pramith M., Sarath N., Arjun Krishna S., Arjun A. Design and fabrication of supercharging an engine using vehicle suspension, Applied Mechanics and Materials, Trans Tech Publ, 2015; 239–245.
39. Jegan C.D., Selvakumaran T., Karthe M., Hemachandu P., Gopinathan R., Sathish T., Ağbulut Ü. Influences of various metal oxide-based nanosized particles-added algae biodiesel on engine characteristics, Energy, 2023; 284: 128633.
40. Kamarulzaman M.K., Hafiz M., Abdullah A., Chen A.F., Awad O.I. Combustion, performances and emissions characteristics of black soldier fly larvae oil and diesel blends in compression ignition engine, Renewable Energy, 2019; 142: 569–580.
41. Ashok B., Nanthagopal K., Vignesh D.S. *Calophyllum inophyllum* methyl ester biodiesel blend as an alternate fuel for diesel engine applications, Alexandria Engineering Journal, 2018; 57: 1239–1247.
42. An H., Yang W., Chou S., Chua K. Combustion and emissions characteristics of diesel engine fueled by biodiesel at partial load conditions, Applied energy, 2012; 99: 363–371.
43. Ağbulut Ü., Karagöz M., Sarıdemir S., Öztürk A. Impact of various metal-oxide based nanoparticles and biodiesel blends on the combustion, performance, emission, vibration and noise characteristics of a CI engine, Fuel, 2020; 270: 117521.
44. Iodice P., Cardone M. Ethanol/gasoline blends as alternative fuel in last generation spark-ignition engines: a review on CO and HC engine out emissions, Energies, 2021; 14: 4034.
45. Nagappan M., Devaraj A., Babu J., Saxena N.V., Prakash O., Kumar P., Sharma A. Impact of additives on Combustion, performance and exhaust emission of biodiesel fueled direct injection diesel engine, Materials Today: Proceedings, 2022; 62: 2326–2331.
46. Huang Z., Huang J., Luo J., Hu D., Yin Z. Performance enhancement and emission reduction of a diesel engine fueled with different biodiesel-diesel blending fuel based on the multi-parameter optimization theory, Fuel, 2022; 314: 122753.
47. Mourad M., Mahmoud K.R., NourEldeen E.-S.H. Improving diesel engine performance and emissions characteristics fuelled with biodiesel, Fuel, 2021; 302: 121097.
48. Razak N.H., Hashim H., Yunus N.A., Klemeš J.J. Reducing diesel exhaust emissions by optimisation of alcohol oxygenates blend with diesel/biodiesel, Journal of Cleaner Production, 2021; 316: 128090.
49. Katal R., Masudy-Panah S., Tanhaei M., Farahani M.H.D.A., Jiangyong H. A review on the synthesis of the various types of anatase TiO_2 facets and their applications for photocatalysis, Chemical Engineering Journal, 2020; 384: 123384.
50. Wold A. Photocatalytic properties of titanium dioxide (TiO_2), Chemistry of Materials, 1993; 5: 280–283.